Elongations of epithelial colony *in vitro*: symmetry breaking through collective effects

Jordi Comelles[1], Soumya SS[2], S. Anvitha[3], Guillaume Salbreux[4], Frank Jülicher[5], Mandar M. Inamdar[2#], Daniel Riveline[1]*

[1]Laboratory of Cell Physics ISIS/IGBMC, CNRS and University of Strasbourg, Strasbourg, France; Institut de Génétique et de Biologie Moléculaire et Cellulaire, Illkirch, France; Centre National de la Recherche Scientifique, UMR7104, Illkirch, France; Institut National de la Santé et de la Recherche Médicale, U964, Illkirch, France; Université de Strasbourg, Illkirch, France.
[2]Department of Civil Engineering, Indian Institute of Technology Bombay, Powai, Mumbai 400076, INDIA.
[3]Department of Mechanical Engineering, Indian Institute of Technology Bombay, Powai, Mumbai 400076, INDIA.
[4]The Francis Crick Institute, 1 Midland Road, London NW1 1AT, United Kingdom.
[5]Max Planck Institute for the Physics of Complex Systems, Nöthnitzer Str. 38, 01187 Dresden, Germany.

Electronic address: #minamdar@iitb.ac.in, *riveline@unistra.fr

Abstract

Tissue elongation is a central morphogenetic event occurring in all organisms in development[1,2]. During this process, symmetry of cells and tissues is broken by different mechanisms, such as neighbor exchange[3,4], cell elongation[5,6] and oriented cell division[7]. While the phenomenon is known to involve remodeling of adherens junctions[4] and acto-myosin[4,8] at the molecular level, mesoscopic mechanisms leading to distinct morphogenesis processes are poorly understood. This is partly because inputs from morphogen gradients[9] or from neighboring tissues[10,11] can affect tissue autonomous self-organization in vivo. *It is therefore difficult to disentangle cell intrinsic from externally mediated behaviors. Here we use* in vitro *experiments and numerical simulations to characterize the spontaneous behavior of a growing cell colony* in vitro. *We show that* in vitro *tissue elongation arises from anisotropy in the average cell elongation. This anisotropy sets the direction along which boundary cells migrate radially resulting in a non-isotropic elongation that arises primarily through cell elongation. For colonies submitted to a time periodic stretch, the axis of global symmetry breaking can be imposed by external force, and tissue elongation arises through oriented neighbor exchange. Emergence of radially migrating cells and the interplay between cell elongation and cell rearrangements are confirmed by numerical simulations based on a vertex model. Our results suggest that spontaneous shape deformation is related to the mean orientation of the nematic cell elongation field in the absence of any external input. This provides a framework to explain autonomous tissue elongation and how contributions from different mesoscopic mechanisms can be modulated by external forces.*

To study the spontaneous tissue deformation arising during epithelial growth, we designed an *in vitro* assay to track symmetry breaking, both spontaneous and driven by external force. We prepared isotropic colonies of Madin Darby Canine Kidney (MDCK) cells, which assume features of epithelial cells *in vivo*[12–14]. The initial size and shape of the colonies were controlled by plating cells in microfabricated circular stencils[15] of 250 µm in diameter (Figure 1a), the

typical coherence length of epithelial tissues[16]. When cells reached confluency, the stencil was removed at t_0. Strikingly, circular colonies were initially surrounded by an acto-myosin cable (Supplementary Figure 1). Cell dynamics was followed over time by phase contrast (Movie 1) or fluorescence microcopy with strains labeled with GFP cadherin (Figure 1b), that allowed to observe the behavior of individual cells. We observed that colonies expanded in a anisotropic manner (Figure 1c).

In order to compare elongations in each experiment, we quantified the breaking of symmetry by ellipse-fitting the colony. Shape change analysis was quantified by a nematic shape elongation tensor $\boldsymbol{Q}$, which has two independent components, $Q_{xx} = ½ \ln(a/b)\cos(2\bullet\theta)$ and $Q_{xy} = ½ \ln(a/b)\sin(2\bullet\theta)$ (Figure 1d, see caption for definitions of a, b, θ). As can be seen in Figure 1e, MDCK colonies elongated persistently along the main axis of elongation ($Q_{xx} > 0$ and $Q_{xy} \approx 0$). We note that elongation observed in 6 hours was similar in magnitude to tissue elongation observed during *in vivo* morphogenesis, for instance in the wing blade in *Drosophila*[11]. Moreover, the elongation direction ($\theta_{\text{final}} = \theta(t = 6\text{ h})$) converges to a constant value within 2 hours after t_0 (Figure 1f).

It has been previously described for *C. elegans* embryo elongation[10] and in other organisms[17] that time periodic stretch can play a role in morphogenesis. Motivated by these observations, we explored whether oscillatory external forces could have an impact on the direction of elongation. We designed an experimental set-up where elongating colonies were submitted to cyclic stretching (Figure 2a and Movie 2). We explored frequencies and extensions around physiological values[17] (see Supplementary Material Section I and Supplementary Figure 2). Among conditions, we observed colony elongation along the direction imposed by the external strain when we stretched cyclically with 60 s timescale and 5% strain (Figure 2b and Movie 3), a response resulting from collective effects (Supplementary Figure 3 and Supplementary Material Section II). The components of the nematic shape elongation tensor $\boldsymbol{Q}$ under cyclic stretching were comparable to the spontaneous elongation of colony when stretch was not applied, but oriented in the direction of external force (Figure 2c and 2d).

We next sought to identify the source of symmetry breaking in both conditions. It has previously been reported that in MDCK monolayers, cells can migrate tangentially to the monolayer boundary when confined[16], or perpendicular to the boundary in the form of multicellular groups or fingers during monolayer expansion[14,18]. During spontaneous elongation of MDCK colonies in the absence of external forces (Movie 4), we observed that boundary cells tend to move either perpendicularly or tangentially to the colony boundary (Figure 3a, Supplementary Figure 4 and Supplementary Material Section III and IV). We observed that the direction of motion of growing fingers consistently corresponded to the colony elongation direction (Figure 3b and 3c). We then measured the position and displacement for each finger in control colonies and colonies under cyclic stretching (Figure 3d). We observed that, when growing parallel to the direction of force application, finger cells performed larger displacements than when growing perpendicularly. To further explore this effect, we grew MDCK monolayers with straight boundaries either parallel or perpendicular to the external force. Then, we let fingers appear and grow for 2 hours before applying cyclic stretching (Figure 3e). When fingers were growing perpendicular to the stretching direction, they shrank upon application of cyclic stretching; in contrast, fingers further elongated when parallel to the direction of external forces. Altogether, this suggests that direction of finger-like structures correlates with elongation direction, and that external stretching affects the dynamics of finger growth.

We then wondered if the process of finger growth is a cause or consequence of the symmetry breaking of the shape of the colony. We observe that when a finger pulls outward on the colony, cells in the immediate vicinity of the finger tend to reorient their elongation axis towards the finger (Figure 4a). Recent studies have shown that the nematic field of cell elongation and its topological defects are involved in the growth of bacterial colonies[19] and in controlling dynamics[20,21], death and extrusion[22] of epithelial cells. We wondered if the spontaneous elongation of colonies would also be related to the average cell elongation. We followed the evolution of the cell elongation nematic field in different colonies during expansion. We first obtained the spatiotemporal cell elongation nematic field **q** (see Supplementary Figure 5 and 6, Movie 5 and Supplementary Material Section V). We could obtain the angle θ_{nematic} of the mean of the nematic field at t_0 which we compared with final colony orientation obtained in the ellipse fitting analysis (Figure 4b, Supplementary Figure 7 and Supplementary Material Section V). Strikingly, we observed a clear average cell elongation even at the time of stencil removal t_0, and the corresponding angle θ_{nematic} correlated with colony orientation when elongation direction is established (Figure 4c, Supplementary Figure 7 and 8). The cell elongation nematic field at t_0 was not typically homogeneous but exhibited a complex pattern with ±½ topological defects (Figure 4b, Supplementary Figure 6 and Supplementary Material Section V). Since the orientation of tissue elongation correlates with orientation of average cell elongation at t_0, this suggests that 'leader' cells pulling outward on the colony are not the primary cause of symmetry breaking in colony shape, but rather follow from the initial cell shape elongation before stencil removal.

We next sought to evaluate quantitatively the contribution of cellular processes to elongation. We isolated the contributions of each cellular event through tissue segmentation, cell tracking and neighbor triangulation[11,23] (see Supplementary Material Section V, Figure 4d and 4e and Movie 6). This procedure decomposes overall tissue elongation, which is quantified in terms of cumulative total pure shear, into contributions from cell elongation and topological changes. Five main events contribute to total shear: cell elongation change, cell division, cell extrusion, T1 transition, and correlation effects[11,23]. At the colony scale, shear decomposition plots (Figure 4f and Supplementary Figure 9) revealed that the total pure shear gives values consistent with elongation estimates from ellipse fitting (Figure 4g). Note that various contributions to shear decomposition exhibit significant variability between experiments (Supplementary Figure 9). However, we found that after the first 2 hours, the contribution of cell elongation is generally comparable to the total pure shear, with a smaller contribution from other sources (Figure 4g). When looking at the shear decompositions of colonies under cyclic stretching (Supplementary Figure 10), the cumulative shear values were also similar to the ones obtained by ellipse fitting (Supplementary Figure 11). Interestingly, we found however that in that case, shear created by T1 transitions is the main contributor for the total pure shear, while cell elongation does not contribute to tissue elongation (Supplementary Figure 10 and 11). This indicates that applying oscillatory forces to the tissue changes fundamentally the main mode of tissue elongation by favouring topological rearrangements of the cell network.

We then asked whether a model could reproduce experimental observations of shear decomposition and, in particular, in which conditions tissue elongation would arise from cell elongation or from topological transitions. We developed a vertex model with addition of a simple set of rules (see Supplementary Material Section VI). We generated a confluent colony of circularly confined cells, in which a unit director **p** that represented the cell polarity was assigned to each cell. Based on orientation of the director, each cell generated an extensile active stress $\boldsymbol{\sigma}_a$ and bias λ in the base value of its edge contractility to promote cell elongation and active T1 transitions. We assumed that the experimentally measured cell elongation

nematic **q** is a readout of the underlying cell polarity **p**. Hence, the initial spatial distribution of **p** was based on the commonly observed pattern of **q** (Figure 4h). To evolve **p** with time, we imposed that **p** of the exterior cells tended to be parallel to the boundary, whereas the inner cells tended to align their **p** with those of their neighbors (Supplementary Material Section VI).

Upon removal of confinement, we found that the simulated colony spontaneously elongates, in a direction set by the orientation of the mean cell elongation nematic field, along with the formation of finger-like structures near the +½ defect, as observed experimentally (see Movie 7). Our simulations therefore reproduce experimental observations indicating that colony deformation can be understood without forces exerted by a leader cell at the colony boundary (Figure 4h, Movie 7, and Supplementary Material Section VI). To test whether we could also recapitulate different contributions of the total pure shear inside the tissue, we performed a shear decomposition analysis of *in silico* Movies. We found a qualitatively similar cumulative shear-strain decomposition as was observed in experiments (Figure 4i), where the main contribution came from cell elongation. Moreover, by changing the relative contributions of the cellular active stress magnitude ($\boldsymbol{\sigma}_a$) and the edge tension bias (λ), we could modulate the relative contributions from cell elongations and T1 transitions to the total pure shear (Supplementary Figure 12 and 13) as was also observed in experiments with colonies in the absence or presence of cyclic stretching (Supplementary Figures 10 and 11). When $\boldsymbol{\sigma}_a$ was dominant, the colony elongation was primarily due to cell elongation, whereas when λ was the stronger term, T1 transitions were the main cause of colony elongation. These results provide possible cellular mechanisms that can affect the process of tissue deformation and influence whether cell elongation, or cellular rearrangements, dominate tissue elongation.

Taken together, we showed that isotropic MDCK colonies spontaneously expanded in an anisotropic manner. Circular colonies have a non-zero average cell elongation even before expansion starts. Orientation of the average cell elongation strongly influences orientation of the final colony shape. Interestingly, we observed that direction of elongation could be rectified by imposing an external cyclic force. Then, finger-like structures seem to drive the asymmetric expansion of the colony by migrating radially, but such expansion could also happen by a concerted effect from all cells by their tendency to align their elongation axis with respect to their neighbors, as seen in simulations. Moreover, this symmetry breaking in the alignment of cell shape would also collectively contribute to the total pure shear.

Our results reinforce the idea that cell elongation nematic field can have an impact on epithelia morphogenesis. It was already shown that topological defects in the cell elongation nematic field have a key role on epithelial dynamics[20] and on cell death and extrusion[22]. Now, we showed that circular epithelial colonies when in confinement build up a mean nematic orientation. This symmetry breaking results from the inner activity of cells, and sets the direction for colony elongation. Changes in epithelial shape could be revisited *in vivo* with this framework. This could potentially reveal generic features of the role of tissue anisotropies in developmental biology.

Acknowledgments

We acknowledge M. Popovic and R. Etournay for stimulating discussions and help with Tissue Miner, J. Nelson, P. Silberzan, S. Coscoy for sharing the MDCK strains, and J. Prost, K. Dayal and M. Zapotocky for helpful suggestions, David Rodriguez and the Riveline Lab.. D.R. and M.M.I. thank MPI-PKS and MPI-CBG for hospitality and many interactions. D.R.

acknowledges support from CNRS (ATIP), ciFRC Strasbourg, the University of Strasbourg, Labex IGBMC, Foundation Cino del Duca. This study with the reference ANR-10-LABX-0030-INRT has been also supported by a French state fund through the Agence Nationale de la Recherche under the frame programme Investissements d'Avenir labelled ANR-10-IDEX-0002-02. M.M.I. acknowledges funding from Department of Biotechnology, Government of India (BT/06/IYBA/2012) and Industrial Research and Consultancy Center (IRCC), IIT Bombay. G.S. was supported by the Francis Crick Institute which receives its core funding from Cancer Research UK (FC001317), the UK Medical Research Council (FC001317), and the Wellcome Trust (FC001317).

Materials and methods

Cell culture. MDCK cells (GFP-E-cadherin strain [13], GFP-Actin strain, RFP-LifeAct / GFP-myosin strain [24]) were cultured in Dulbecco's modified Eagle medium (D-MEM) 1g/l glucose (Invitrogen), supplemented with 10% fetal bovine serum (FBS) (Invitrogen) and 1% penicillin-streptomycin (and the corresponding resistance for each strain). Cells were passaged every 2-3 days using standard procedures.

Fabrication of PDMS membranes and stencils. Poly(dimethylsiloxane) (PDMS) (Sylgard) was prepared by mixing the pre-polymer and the cross-linker at a 10:1 ratio. To prepare stretchable membranes, uncured PDMS was first centrifuged (3000 rpm for 5 min) to remove air bubbles. Afterwards, the PDMS was spin coated on a flat polystyrene (PS) surface (500 rpm for 1 min) and cured at 65ºC overnight. PDMS stencils were prepared as described previously [15]. Briefly, SU-8 2050 molds containing circles of 250 µm in diameter were prepared by standard photolithography. Uncured PDMS was then spin-coated on molds to a thickness lower than the height of the microstructures (50 µm) and cured overnight at 65ºC. Stencils for the finger experiments were prepared by spin-coating uncured PDMS on a flat surface.

Cell seeding on stencils. The PDMS stencils were cut, peeled off the mold, and placed in a 2% Pluronic F-127 (Sigma-Aldrich) in PBS for 1 h. The stencils were then kept in PBS for 2h and dried under the hood flow. PDMS stretchable membranes were cut and then activated using O_2 plasma. The membranes and the stencils were exposed to UV light in the cell culture hood for 10 min. Afterwards, stretchable membranes were incubated with fibronectin 20 µg/ml for 1 h, rinsed with PBS and dried. PDMS membranes were placed on a PS holder, and the PDMS stencils were deposited on top of the membrane right after. A rectangular PDMS chamber was attached onto the membrane using vacuum grease, and cells were seeded at a density of 20000 cells/mm^2 [25] for 4 h. When cells were attached, the medium was changed and the membrane with the cells was kept in the incubator. Local cell density could vary within each colony. We followed the dynamics of assembly of the colony prior removal of the stencil and we could see that cellular clusters size distribution and respective location within the cavity at plating could contribute to these variations. Once they formed confluent circular colonies, the stencils were removed with tweezers carefully before starting the experiment. Some of the colonies exhibited elongation in the short time window between stencil removal and the start of image acquisition.

Time-lapse microscopy. After stencil removal, the medium was replaced by L-15 (Leibovitz's L-15 medium, Invitrogen) supplemented with 10% FBS. Cells were then observed under a Nikon Ti inverted microscope using either a x10 or a x20 objective for 6 h at 37ºC. Images were acquired every 5 min.

Stretching experiments. The stretching device was designed in the lab. Briefly, a Thorlabs motor (Thorlabs z812 motor, Thorlabs) was controlling the motion of a PDMS membrane, and everything was mounted on a custom-made microscope stage. Circular colonies were plated on PDMS membranes, and after removal of the stencils, samples were placed on the microscope. Cyclic stretches were applied and images were taken every 30 minutes typically shortly to prevent interfering with the time course of the experiments. We probed 3 times for cycles, 20s, 60s, 120s, and 3 extensions, 5%, 10%, and 20%. The shape of the cycles was triangular. We checked that the PDMS stencils were elastic at all extension and frequency ranges.

Chemical treatments. To prevent the formation of E-cadherin-mediated adhesion, cells were incubated for 30min with L-15 medium containing 5 mM EDTA (Sigma-Aldrich) and 10 µg/ml anti-E-cadherin blocking antibody that targeted the extracellular domain of E-cadherin[26] (uvomorulin, monoclonal anti-E- cadherin antibody, Sigma); after incubation, the medium was replaced by normal L-15 and the experiment started.

Finger dynamics experiments. For the finger test after growth, we let finger grow for 2 hours, and we subsequently applied the cyclic stretch.

Colony shape change analysis. Shape change analysis was performed using ImageJ (http://rsb.info.nih.gov/ij, NIH). The outline of the colony on phase contrast images was ellipse fitted at every time point. Major axis a, minor axis b, and ellipse orientation θ were obtained. We computed $\boldsymbol{Q}$, defined as $Q_{xx}(t) = \frac{1}{2}\ln(a(t)/b(t))\cdot\cos 2\cdot(\theta(t) - \theta(t_{final}))$ and $Q_{xy}(t) = \frac{1}{2}\ln(a(t)/b(t))\cdot\sin 2\cdot(\theta(t) - \theta(t_{final}))$ to quantify cell colony elongation. In stretching experiments, the x axis corresponds to the direction of the external stretch and $\boldsymbol{Q}$ components are defined as $Q_{xx}(t) = \frac{1}{2}\ln(a(t)/b(t))\cdot\cos 2\cdot(\theta(t))$ and $Q_{xy}(t) = \frac{1}{2}\ln(a(t)/b(t))\cdot\sin 2\cdot(\theta(t))$.

Velocity analysis. The centroid trajectories of cells were tracked using the manual tracking plug-in in ImageJ. Data analysis was performed using a custom-made code in MATLAB (The MathWorks). Cell positions were characterized by a vector $\mathbf{r}(t)$, with t denoting time and $\mathbf{r}$ position in space (bold letter refers to a vector). Every recorded cell position during the time-lapse experiment was defined as $\mathbf{r}_i = \mathbf{r}(t_i)$, where $t_i = i\Delta t$ are the times of recording and Δt denotes the duration of time-lapses. The average velocity of each cell was then defined as $v = (1/T)\cdot\sum_i r_i$, being r_i the module of the vector $\mathbf{r}_i$ and T the total duration of the trajectory.

Colony segmentation and cell tracking. Movies acquired using a MDCK GFP-E-cadherin strain were first pre-processed with FIJI. The *subtract background* function was applied to remove noise. Images were then loaded to Tissue Analyzer (TA) v8.5 [27] for edge detection and cell tracking.

Topological Defects. The processed time-lapse movies of expanding colonies were subjected to analysis with the OrientationJ plugin of FIJI to produce the smoothed director field representing cell-shape anisotropy. The resulting director field was further quantified by studying the spatiotemporal evolution of ±1/2 topological defects that were obtained by calculating the winding number over cells of the underlying grid. The smoothing of the underlying Gaussian kernel is approximately of the size of cells and ensured that the most robust defects were observed. The validity of this procedure was cross-verified with the smoothed cell-shape nematic field and the corresponding ±½ defects from the segmented and triangulated data of the experiments processed in TM (Supplementary Figure 5 and Supplementary Material Section V). Finally, the orientation of mean cell-shape nematic calculated at 0 hrs was compared

with shape orientation of the colony at t = 2 hrs. See Supplementary Material Section V for more details (also see Movie 7).

Quantification of cellular deformations, topological transitions and their contribution to pure shear deformation. After obtaining the geometrical and topological information of the colonies from the series tracked images generated using TA, TM was used to extract, triangulate and store the data with the help of an automated workflow. The database obtained after this stage of analysis was used to quantify various state properties such as cell area, neighbor number, cell elongation and the contribution of different cellular processes to deformation using scripts written both in *R* and in *Python*. TM was further used to quantify the contributions of various cellular events such as cell elongation and topological transitions to the colony deformation. More details about this analysis can be found in Supplementary Material Section V (also see Movie 6).

Vertex Model Simulations. A vertex model was developed with an addition of a unit nematic director **p** to every cell. The orientation of the boundary cell **p** was maintained parallel to the boundary, whereas **p** for internal cells were modeled to have a tendency to align with the **p** of its neighbors. In these simulations, an extensile active stress $\sigma_a(\mathbf{pp}-\frac{1}{2}\mathbb{1})$ acts to increase cell elongation along **p**. In addition, a bias λ was also applied on the basic edge tension with respect to the director **p** of its neighboring cells. This bias reduces (increases) the tension of the edge along (perpendicular to) **p**. Consequently, the closure (formation) of edges is enhanced in the direction perpendicular (parallel) to **p**. Hence, the T1 transitions in the region around the cells are oriented to cause shear elongation (contraction) along (perpendicular) to **p**. The colony is provided with an initial condition for **p** that mimics the initial configuration of many experimentally observed cell shape nematic field **q** with two +½ defects that are separated by a distance. To begin with, the cell positions and director orientations were evolved under colony confinement till cell position and **p** do not change significantly. The confinement is then removed to see how the colony breaks symmetry in its shape. In another set of simulations, a small motility v_0 was also provided to the internal cells (Supplementary Figure 13). Similar to the experiments, the output of these simulations was also processed in TM and analyzed for topological defects and pure shear decomposition. More details of the simulations are provided in Supplementary Material Section VI (also see Movie 7).

References

1. Guillot, C. & Lecuit, T. Mechanics of Epithelial Tissue Homeostasis and Morphogenesis. *Science* **340**, 1185–1189 (2013).
2. Lecuit, T. & Lenne, P.-F. Cell surface mechanics and the control of cell shape, tissue patterns and morphogenesis. *Nat Rev Mol Cell Biol* **8**, 633–644 (2007).
3. Rauzi, M., Verant, P., Lecuit, T. & Lenne, P.-F. Nature and anisotropy of cortical forces orienting Drosophila tissue morphogenesis. *Nat. Cell Biol.* **10**, 1401–10 (2008).
4. Rauzi, M., Lenne, P.-F. & Lecuit, T. Planar polarized actomyosin contractile flows control epithelial junction remodelling. *Nature* **468**, 1110–4 (2010).
5. Clarletta, P., Ben Amar, M. & Labouesse, M. Continuum model of epithelial morphogenesis during caenorhabditis elegans embryonic elongation. *Philos. Trans. R. Soc. A Math. Phys. Eng. Sci.* **367**, 3379–3400 (2009).
6. Vuong-Brender, T. T. K., Yang, X. & Labouesse, M. Chapter Thirty-Five - C. elegans Embryonic Morphogenesis. in *Essays on Developmental Biology, Part A* (ed. Wassarman, P.) **116**, 597–616 (Academic Press, 2016).
7. Campinho, P. *et al.* Tension-oriented cell divisions limit anisotropic tissue tension in

epithelial spreading during zebrafish epiboly. *Nat. Cell Biol.* **15**, 1405–14 (2013).
8. He, L., Wang, X., Tang, H. L. & Montell, D. J. Tissue elongation requires oscillating contractions of a basal actomyosin network. *Nat. Cell Biol.* **12**, 1133–42 (2010).
9. Gilmour, D., Rembold, M. & Leptin, M. From morphogen to morphogenesis and back. *Nature* **541**, 311–320 (2017).
10. Zhang, H. *et al.* A tension-induced mechanotransduction pathway promotes epithelial morphogenesis. *Nature* **471**, 99–103 (2011).
11. Etournay, R. *et al.* Interplay of cell dynamics and epithelial tension during morphogenesis of the Drosophila pupal wing. *Elife* **4**, 1–51 (2015).
12. Reinsch, S. & Karsenti, E. Orientation of Spindle Axis and Distribution of Plasma Membrane Proteins during Cell Division in Polarized MDCKII Cells. *J. Cell Biol.* **126**, 1509–1526 (1994).
13. Adams, C. L., Chen, Y.-T., Smith, S. J. & James Nelson, W. Mechanisms of Epithelial Cell–Cell Adhesion and Cell Compaction Revealed by High-resolution Tracking of E-Cadherin– Green Fluorescent Protein. *J. Cell Biol.* **142**, 1105–1119 (1998).
14. Reffay, M. *et al.* Interplay of RhoA and mechanical forces in collective cell migration driven by leader cells. *Nat. Cell Biol.* **16**, 217–23 (2014).
15. Ostuni, E., Kane, R., Chen, C. S., Ingber, D. E. & Whitesides, G. M. Patterning Mammalian Cells Using Elastomeric Membranes. *Langmuir* **16**, 7811–7819 (2000).
16. Doxzen, K. *et al.* Guidance of collective cell migration by substrate geometry. *Integr. Biol.* **5**, 1026–1035 (2013).
17. Zhang, H. & Labouesse, M. Signalling through mechanical inputs - a coordinated process. *J. Cell Sci.* **125**, 3039–3049 (2012).
18. Reffay, M. *et al.* Orientation and polarity in collectively migrating cell structures: statics and dynamics. *Biophys. J.* **100**, 2566–75 (2011).
19. Doostmohammadi, A., Thampi, S. P. & Yeomans, J. M. Defect-Mediated Morphologies in Growing Cell Colonies. *Phys. Rev. Lett.* **117**, 1–5 (2016).
20. Kawaguchi, K., Kageyama, R. & Sano, M. Topological defects control collective dynamics in neural progenitor cell cultures. *Nature* **545**, 327–331 (2017).
21. Mueller, R., Yeomans, J. M. & Doostmohammadi, A. Emergence of Active Nematic Behavior in Monolayers of Isotropic Cells. *Phys. Rev. Lett.* **122**, 48004 (2019).
22. Saw, T. B. *et al.* Topological defects in epithelia govern cell death and extrusion. *Nature* **544**, 212–216 (2017).
23. Etournay, R. *et al.* TissueMiner: A multiscale analysis toolkit to quantify how cellular processes create tissue dynamics. *Elife* **5**, 1–28 (2016).
24. Klingner, C. *et al.* Isotropic actomyosin dynamics promote organization of the apical cell cortex in epithelial cells. *J. Cell Biol.* **207**, 107–21 (2014).
25. Serra-Picamal, X. *et al.* Mechanical waves during tissue expansion. *Nat. Phys.* **8**, 628–634 (2012).
26. Gumbiner, B., Stevenson, B. & Grimaldi, A. The role of the cell adhesion molecule uvomorulin in the formation and maintenance of the epithelial junctional complex. *J. Cell Biol.* **107**, 1575–1587 (1988).
27. Aigouy, B. *et al.* Cell Flow Reorients the Axis of Planar Polarity in the Wing Epithelium of Drosophila. *Cell* **142**, 773–786 (2010).

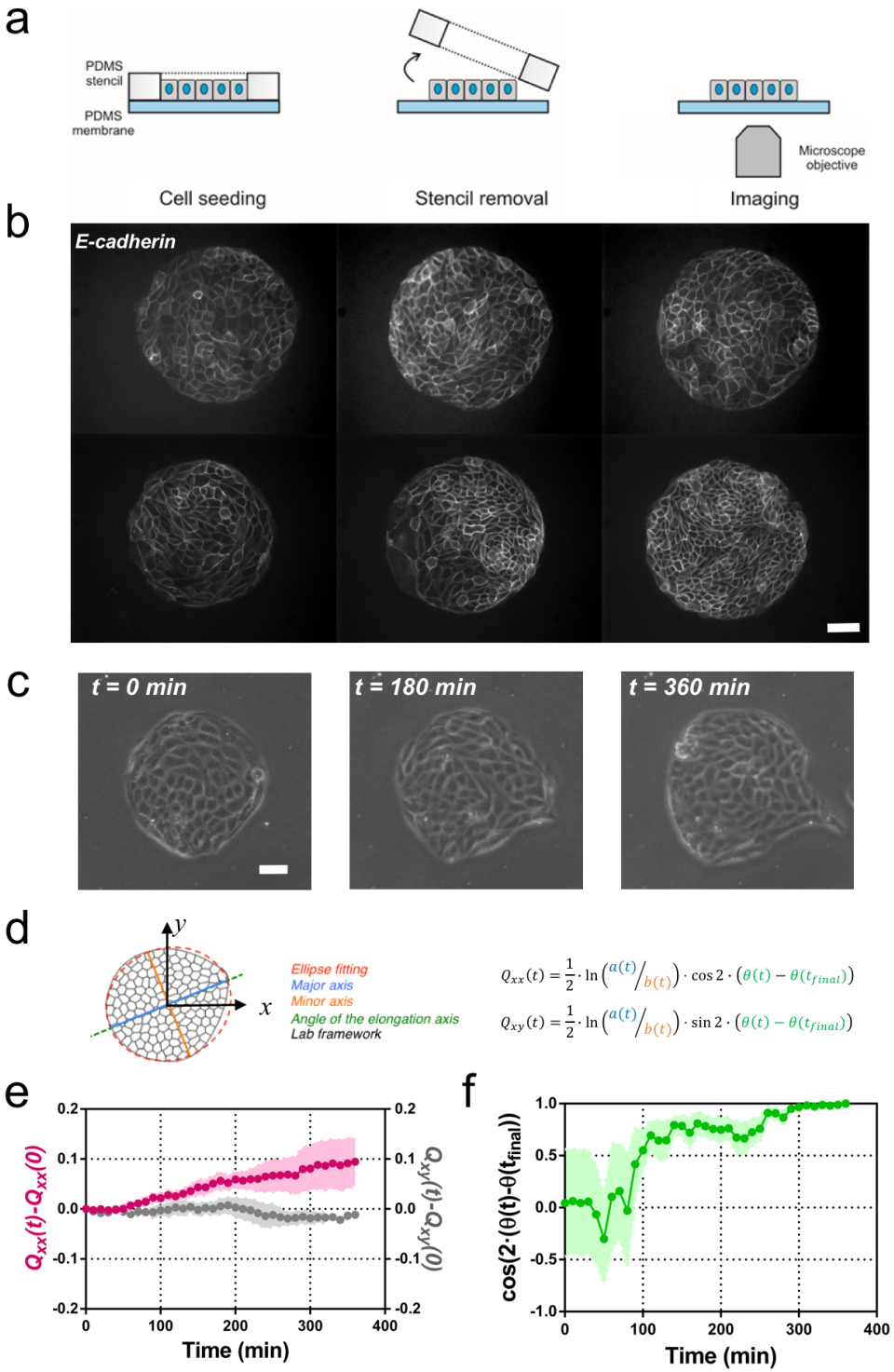

Figure 1. **Symmetry breaking and its quantification**. (**a**) Schematics of the experimental set-up: MDCK cells were seeded on a PDMS membrane using stencils to predefine their shape. When the colony was confluent, the stencil was removed and the expansion of the colony was observed under the microscope. (**b**) Several examples of MDCK colonies (GFP-E-cadherin) after stencil removal and prior to colony expansion. Scale bar 50 µm. (**c**) Phase contrast images of the spontaneous elongation of a MDCK colony for 360 min. Scale bar 50 µm. (**d**) Colony elongation is quantified by ellipse fitting and Q_{xx} and Q_{xy} evaluation referred to the elongation axis. (**e**) Q_{xx} (left y axis) and Q_{xy} (right y axis) during 360 min of colony expansion. Mean value ± standard error of the mean, N = 4 independent experiments. (**f**) Cosine of two times the angle difference between the instantaneous main direction of the colony (θ(t)) and the main direction

of the colony at 360 min ($\theta(t_{final})$). Colonies set the elongation direction within the first 120 min. Mean value ± standard error of the mean, N = 4 independent experiments.

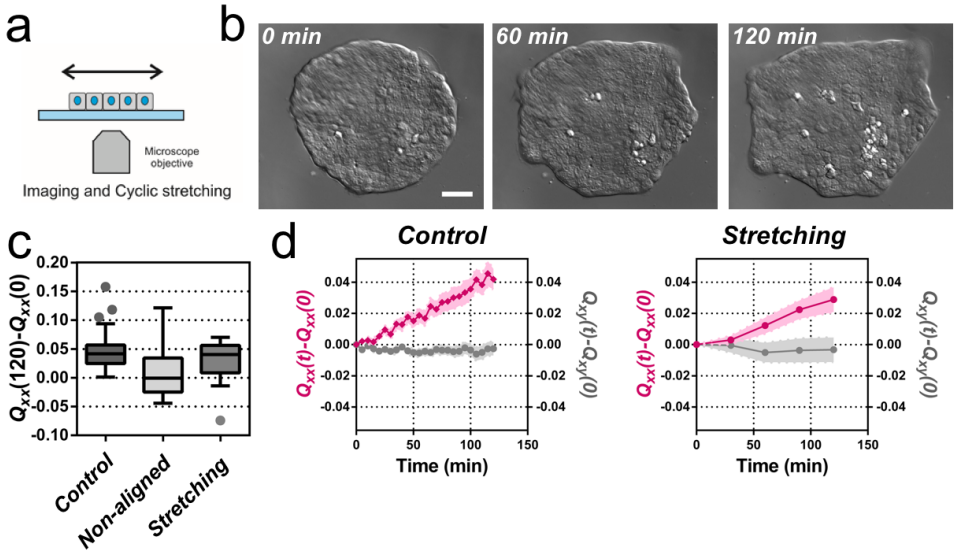

Figure 2. **Cyclic stretching rectifies symmetry breaking.** (**a**) Schematics of the experiment where the colony expansion was observed under the microscope while the underlying membrane was stretched. (**b**) Snapshots of the expansion of a MDCK colony while cyclically stretched. Scale bar 50 µm. (**c**) Colony elongation (Q_{xx}) of control colonies along the elongation axis, control colonies in the laboratory framework (non-aligned) and colonies under cyclic stretching in the laboratory framework (stretching). Tukey's box plot, $N_{control} \geq 3$ independent experiments, n = 25 colonies and $N_{stretching} \geq 3$, n = 20 colonies. Mann-Whitney test control *vs* control aligned p = 0.0003, control *vs* stretching p = 0.0281 and control aligned *vs* stretching p = 0.3319. (**d**) Q_{xx} (left y axis) and Q_{xy} (right y axis) during 120 min of colony expansion for control colonies and colonies under cyclic stretching. Mean value ± standard error of the mean, $N_{control} \geq 3$, n = 14 colonies and $N_{stretching} \geq 3$, n = 20 colonies.

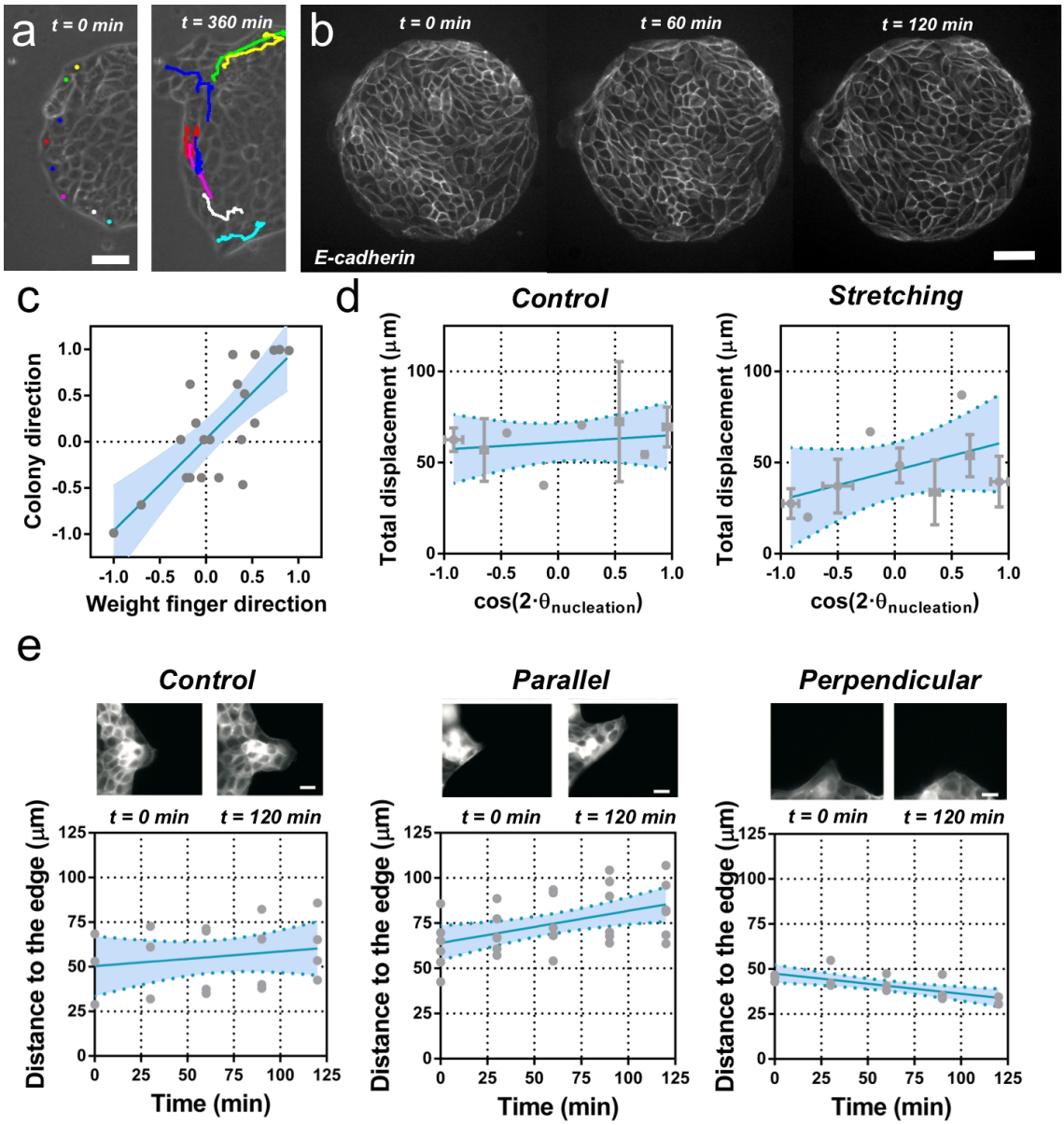

Figure 3. **Fingers and symmetry breaking**. (**a**) Trajectories of boundary cells during colony expansion. Two types of trajectories are observed: radial and tangential. Scale bar 50 μm. (**b**) Fluorescent images (GFP-E-cadherin) of a colony evolving for 120 min. Scale bar 50 μm. (**c**) Direction of the colony elongation (quantified by the cosine of 2 times the angle of the main axis of the colony at t = 2 hours) as a function of the weight finger direction (quantified by the average of the cosine of 2 times the angle of each finger trajectory, e.g. the angle corresponding to the vector between the position of the finger at t = 0 hours and t = 2 hours, of each finger weight by the finger's displacement). $N \geq 3$, $n_{colonies} = 12$ colonies and $n_{finger} = 21$ fingers. Blue dashed-line corresponds to the linear fitting of the data points and the shadowed area corresponds to the 95% confidence interval. Pearson's correlation coefficient r = 0.6556, p = 0.0013. (**d**) Total displacement of finger growth as a function of its initial position in the colony (angular coordinate from the center of the colony) for control colonies and colonies under stretching. $N \geq 3$ independent experiments, $n_{colonies} = 11$ colonies and $n_{finger} = 21$ fingers (control) and $N \geq 3$, $n_{colonies} = 10$ colonies and $n_{finger} = 28$ fingers (stretching). Blue lines correspond to linear fitting of data points and the shadowed area corresponds to 95% confidence interval. (**e**) Distance between the tip of the finger and the edge of the monolayer along time, for monolayers

in control conditions, stretched parallel and perpendicular to the finger growth direction. $N \geq 3$ independent experiments for the three conditions and $n = 4$, 6 and 3 fingers respectively. Blue lines correspond to the linear fitting of data points and the shadowed area corresponds to 95% confidence interval.

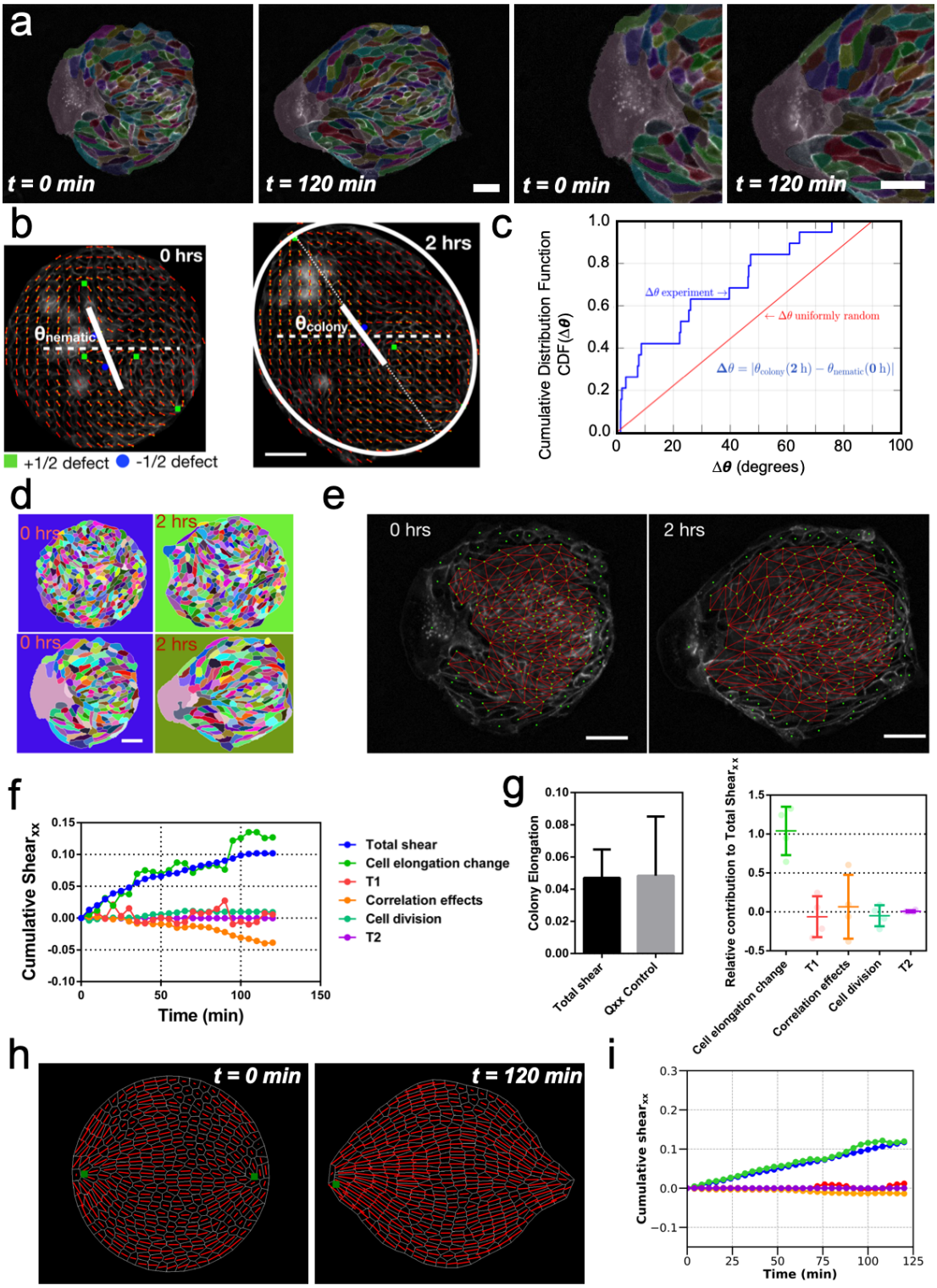

Figure 4. **Collective effects and symmetry breaking**. (**a**) A leader cell at the boundary of the colony pulls the colony outwards while inner cells deform and elongate. Scale bar 50 μm. (**b**) Cell shape is quantified using a nematic field (red segments). First, the mean cell shape nematic is quantified at the moment of stencil removal (0 hours) and the orientation $\theta_{nematic}$ of its mean for the entire colony is obtained. Then, the overall shape of the colony after 2 hours is obtained by fitting an ellipse, whose major axis makes an angle θ_{colony}. The yellow directors correspond to fits for the cell shape nematic field obtained with respect to the +1/2 and -1/2 topological defects of the experimentally obtained (red) nematic field (also see Supplementary Material

Section V for details.) Scale bar 50 µm. (**c**) The cumulative distribution function (CDF) for the difference $\Delta\theta$ between $\theta_{nematic}$ (0 hours) and θ_{colony} (2 hours) is obtained N = 19 colonies. This plot shows a strong correlation between the cell shape nematic and the overall shape symmetry breaking (also see Supplementary Material Section V and Supplementary Figure 7 for details). (**d**) Snap-shots of two colonies from control condition segmented and tracked for cells using Tissue-Analyzer (TA) for a duration of t = 120 minutes starting from removal of stencil at $t = 0$. Scale bar 50 µm. (**e**) The segmented and tracked images are triangulated in Tissue-Miner (TM). Scale bar 50 µm. The green dots represent the centers of the segmented cells. (**f**) The dynamics of triangulation is analyzed in TM to provide the overall xx component of cumulative pure shear strain in the sample colony shown in (b) as a function of time (total shear). The decomposition of total pure shear into different components is also shown (see Supplementary Material Section V). (**g**) Comparison between the mean total pure shear obtained from TM and the overall colony pure shear obtained from ellipse fitting (left) and relative contribution of the different processes to the total pure shear. $N \geq 2$, $n_{colonies} = 4$ colonies. (**h**) A vertex model with internal activity arising from extensile active cell stress and biased edge tension for the cell-cell junctions (see Materials and Methods, Supplementary Material Section VI and Supplementary Figure 12c), shows shear decomposition (**i**) which is similar to its experimental counterpart in (f).